Liu et al. PhotoniX (2022) 3:1
https://doi.org/10.1186/s43074-022-00047-3

PhotoniX

RESEARCH Open Access

Biomimetic sapphire windows enabled by inside-out femtosecond laser deep-scribing

Xue-Qing Liu[1], Yong-Lai Zhang[1*], Qian-Kun Li[1], Jia-Xin Zheng[1], Yi-Ming Lu[1], Saulius Juodkazis[2,3], Qi-Dai Chen[1*] and Hong-Bo Sun[1,4*]

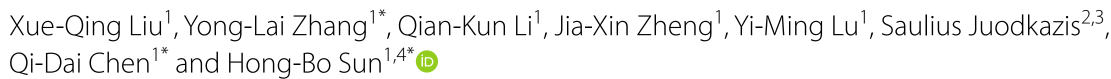

*Correspondence: yonglaizhang@jlu.edu.cn; chenqd@jlu.edu.cn; hbsun@tsinghua.edu.cn
[1] State Key Laboratory of Integrated Optoelectronics, College of Electronic Science and Engineering, Jilin University, Changchun 130012, China
[4] State Key Laboratory of Precision Measurement Technology and Instruments, Department of Precision Instrument, Tsinghua University, Haidian, Beijing 100084, China
Full list of author information is available at the end of the article

Abstract

Femtosecond laser machining of biomimetic micro/nanostructures with high aspect ratio (larger than 10) on ultrahard materials, such as sapphire, is a challenging task, because the uncontrollable surface damage usually results in poor surface structures, especially for deep scribing. Here, we report an inside-out femtosecond laser deep scribing technology in combination with etching process for fabricating bio-inspired micro/nanostructures with high-aspect-ratio on sapphire. To effectively avoid the uncontrollable damage at the solid/air interface, a sacrificial layer of silicon oxide was employed for surface protection. High-quality microstructures with an aspect ratio as high as 80:1 have been fabricated on sapphire surface. As a proof-of-concept application, we produced a moth-eye inspired antireflective window with sub-wavelength pyramid arrays on sapphire surface, by which broadband (3–5 μm) and high transmittance (98% at 4 μm, the best results reported so far) have been achieved. The sacrificial layer assisted inside-out femtosecond laser deep scribing technology is effective and universal, holding great promise for producing micro/nanostructured optical devices.

Keywords: Femtosecond laser, Etching, Antireflection, Biomimetic microstructures, Sapphire

Introduction

Femtosecond laser micromachining has been widely recognized as a versatile tool for fabricating three-dimensional (3D) micro/nanostructures towards biomimetic applications in micro-optics, microfluidics, functional surfaces with super wettability and bioinspired microrobots, etc. [1–8] Nevertheless, to realize 3D fabrication, femtosecond laser micromachining has to perform a point-by-point multi-layer scanning process. In the case of high fluence laser ablation, plenty of fragments and particles would be generated during the multi-layer scanning, [9, 10] which hinders the subsequent deep ablation due to the light scattering and shading. Consequently, high fluence laser ablation usually causes serious damage to solid surface, resulting in low precision and poor surface quality [11]. Nowhere is this more obvious than in the case of deep scribing, where there is a need to produce microstructures with high aspect ratio.

To get precise control over the surface morphology of ultrahard materials (e.g., sapphire and diamond), femtosecond laser modification in combination with subsequent

Springer Open

© The Author(s) 2022. **Open Access** This article is licensed under a Creative Commons Attribution 4.0 International License, which permits use, sharing, adaptation, distribution and reproduction in any medium or format, as long as you give appropriate credit to the original author(s) and the source, provide a link to the Creative Commons licence, and indicate if changes were made. The images or other third party material in this article are included in the article's Creative Commons licence, unless indicated otherwise in a credit line to the material. If material is not included in the article's Creative Commons licence and your intended use is not permitted by statutory regulation or exceeds the permitted use, you will need to obtain permission directly from the copyright holder. To view a copy of this licence, visit http://creativecommons.org/licenses/by/4.0/.

etching technology has been proven an effective solution to reach this end [12–17]. The etching-assisted laser machining technology does not need to undergo intense laser ablation process, it achieves potential microstructures through laser modification. And the removal of materials resorts to subsequent etching process. In this case, inside-out laser machining can be implemented to prepare 3D microstructures, for instance complex microfluidic channel networks. The superiority of this method has been proven in pioneer works with respect to the processing of photosensitive glass, fused silica, et al. For example, Hu et al. have successfully realized complex optofluidic systems inside photosensitive glass by this method [12]. First, 3D modified patterns are designed and fabricated by low-intensity laser scanning from the internal to the surface of the hard materials [18]. Since the laser modified region shows much higher etching rate than the original materials, any desired microstructures can be fabricated by subsequent wet etching or dry etching process. However, in the case of biomimetic fabrication based on ultrahard materials, the etching-assisted laser fabricating usually cannot get precise control of the surface morphology [19]. Since the internal damage threshold is always larger than that at the solid-air interface, uncontrollable surface damage is generally inevitable when the laser scanning path approaches the surface. As a result, plenty of particles, fragments and wrinkles will be generated on the surface, which significantly limits the applications of femtosecond laser in developing delicate biomimetic microstructures. This issue has motivated considerable efforts to develop improved laser micromachining technologies, whereas it remains a big challenge at present.

Here, we proposed an inside-out femtosecond laser deep scribing technology for fabricating biomimetic sapphire window with microstructures on the surface. To effectively avoid the surface and internal damage competition, a silicon oxide (SiO_2) with a reasonable thickness is employed as surface sacrificial layer to ensure high-quality and high-aspect-ratio structuring. Specifically, the uncontrollable damage to the surface can be well restricted within the sacrificial layer. Since the SiO_2 sacrificial layer and the laser modified sapphire region can be easily removed in the subsequent wet etching process using hydrofluoric acid (HF), biomimetic microstructures with delicate surface morphologies and aspect-ratio as high as 80:1 have been successfully fabricated. Inspired by the infrared light antireflection properties of moth compound eyes, we designed and fabricated the sub-wavelength truncated pyramid array structures on both sides of a sapphire window. In the antireflective tests of infrared rays (IR), it demonstrated broadband (3–5 μm) and high transmittance (98% at 4 μm) for normal incidence.

Experimental section

To modify the samples, we used a femtosecond laser with wavelength of 343 nm, which is delivered by third harmonic generation system (Pharos, Light Conversion Ltd). The repetition rate of femtosecond laser is 200 kHz and the pulse width is 290 fs. The samples were fixed on a high-precision three-dimensional nanoscale positioning platform (PI, E-727.3CDA). Then, the laser beam was focused in the samples by an objective lens (Nikon 20×) with numerical aperture of 0.75. In this way, by moving the platform that can be controlled by computer aided design (CAD), three-dimensional micro/nanostructures can be realized via femtosecond laser modification. Then, wet etching was carried out by using 10% HF aqueous solution to remove the sacrificial layer of SiO_2 and

the laser modified regions in sapphire (Hefei Kejing Material Technology, Ltd., thickness of 430 μm). The etching time depends on the depth of the structures. Dry etching process for fabrication of antireflective microstructures was carried out by an inductively coupled plasma system (ICP-100A, Tailong Electronics, Ltd). The etching power was controlled to 600 W of antenna RF power and 300 W of bias RF power. The etching time was 5 min. Chlorine (Cl_2) and boron trichloride (BCl_3) were chosen as the etching gas with flow rates of 20 and 30 sccm. Field-emission scanning electron microscopy (FE-SEM, JEOL JSM-6700F, Japan) was used to show the surface morphology and cross-section of the fabricated microstructures. The three-dimensional morphologies of the antireflective microstructures were measured by laser scanning confocal microscopy (LSCM, OLS4100, Japan). The transmittance of sapphire with antireflective microstructures was investigated using Fourier transform infrared (FTIR) spectrometry.

Results and discussion

Generally, the femtosecond laser pulse exhibits a Gaussian distribution of intensity. To fabricate deep microstructures with high aspect ratio on sapphire, focused laser spot has to scan from inside to outside gradually. Such an inside-out processing can avoid the scattering effect caused by the surface damage, and thus guarantee high resolution and surface smoothness. Nevertheless, when the laser fluence at the focus center reaches the internal damage threshold of sapphire, the laser fluence beyond the central region may exceed the surface damage threshold, since the damage threshold at the solid/air interface is always much lower than that inside the bulky material. As a result, the sapphire surface is more vulnerable to damage when scanning the laser focus from inside to out, especially approaching the surface. To demonstrate this effect clearly, we stimulate the intensity distribution of a laser focus underneath the solid surface, as shown in Fig. 1. Due to the difference in surface and internal damage threshold, uncontrollable damage is always inevitable at the solid-air interface. Consequently, an undamaged.

region with a certain depth (denoted as *dz*) usually forms underneath the surface damages (Fig. 1a). The uncontrollable surface damages lead to poor surface morphology, and the undamaged region underneath the surface may also prevent the subsequent etching process. The combined effects make it challenging to prepare delicate biomimetic microstructures. To get deep insight into the depth of undamaged region, we stimulate the dependance of *dz* on the laser fluence. Generally, the Gaussian light intensity of a femtosecond laser can be described by the following formula:

$$I = \frac{{A_0}^2}{{\omega_z}^2}\exp\left(\frac{-2r^2}{{\omega_z}^2}\right) \tag{1}$$

with

$$\omega_z = \omega_0\sqrt{1+\left(\frac{\lambda z}{\pi {\omega_0}^2}\right)^2} \tag{2}$$

where A_0/ω_z is the amplitude of the electric vector at different position of z axis, r is the perpendicular distance to z axis, λ is the wavelength, and ω_0 is the waist radius at

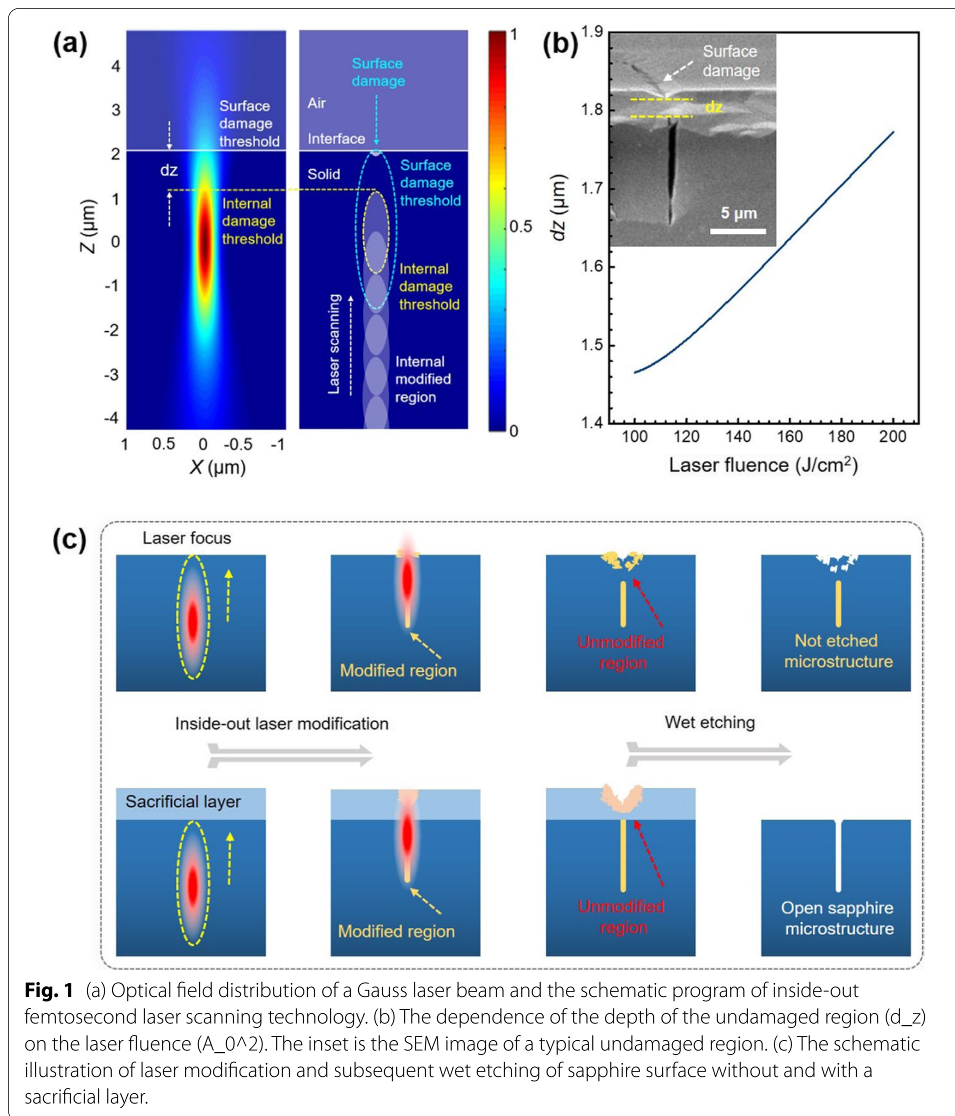

Fig. 1 (a) Optical field distribution of a Gauss laser beam and the schematic program of inside-out femtosecond laser scanning technology. (b) The dependence of the depth of the undamaged region (d_z) on the laser fluence (A_0^2). The inset is the SEM image of a typical undamaged region. (c) The schematic illustration of laser modification and subsequent wet etching of sapphire surface without and with a sacrificial layer.

$z=0$. Then, the distance (d_z) between surface damage threshold I_1 and internal damage threshold I_2 can be described by the following formula:

$$d_z = \frac{\pi\omega_0^2}{\lambda}\left(\sqrt{\frac{A_0^2}{I_2}-1}-\sqrt{\frac{A_0^2}{I_1}-1}\right) \tag{3}$$

The relationship of d_z and A_0^2 is shown in Fig. 1b, in which dz increases with the laser fluence, following a quasi-linear relationship. SEM image (inset of Fig. 1b) confirms the presence of such an undamaged region even after HF etching.

To address this issue, we proposed a sacrificial layer-assisted laser micromachining strategy. Figure 1c shows the comparison of the laser processing and subsequent etching process with and without the sacrificial layer. Generally, the femtosecond laser irradiation can induce the phase change of sapphire from crystalline phase to amorphous/polycrystalline phase, and the laser modified region can be rapidly etched away by HF

solution with the etching selectivity over 104 [7]. In a typical laser processing experiment, the laser fluence can be tuned slightly larger than the phase change threshold of sapphire. The presence of sacrificial layer (here we use SiO_2) with a suitable thickness generate a new air/SiO_2 two-phase interface instead of the air/sapphire interface, which effectively avoids the surface damage at the sapphire. Thus, the undamaged region appears in the SiO_2 sacrificial layer, which can be removed during HF etching. In this way, the desired microstructures with high aspect ratio and good surface quality can be readily prepared (Fig. 1c).

To clarify the fundamental of the formation of undamaged regions in sapphire, we fabricated a series of single-line grooves by varying the depth of the laser focus, and systematically investigated the dependence of the depth and width of the grooves on the relative position of the laser focus to the sapphire surface. Figure 2a shows the scheme of the laser focus depth and the profile SEM image of the resultant micro-grooves fabricated. Notably, when the laser is focused outside the sapphire, surface damage can be induced providing the laser intensity at the solid-air interface reach the damage threshold of sapphire. In this condition, the as-formed grooves are relatively shallow. When the laser focus is tuned downward gradually, both the depth and the width of the grooves are increased. Nevertheless, when the laser is focused underneath the sapphire surface, further increase of the laser focus depth would not increase the size of the grooves, since the as-formed surface damages prevent the deep scribing of sapphire. In this condition, the laser fluence of the focus edge reached the damage threshold of sapphire at the solid-air interface, and the center of laser focus reach the damage threshold of bulky sapphire, while the intensity under the surface damage and far from the focus center is below the damage threshold. As a result, an undamaged region appears underneath the grooves. When the laser focus was assigned deep inside the sapphire, only inside damage was formed, and the surface keeps smooth. The profile SEM image of these grooves (after HF etching) confirms evolution of the profile structures. Figure 2b shows the dependence of the profile morphologies of the grooves on relative depth of laser focus. The depth and width of the grooves first increased with laser focus depth following the same tendency. When they reach a maximum value, the depth and width decreased due to the formation of undamaged region underneath the grooves. In this case, deep scribing of sapphire will be suppressed in the presence of undamaged region.

To realize deep scribing of sapphire, we have to avoid the formation of uncontrollable surface damages and the undamaged region underneath. In this work, we proposed a sacrificial layer-assisted laser micromachining strategy. A SiO_2 film with a suitable thickness was employed as a sacrificial layer on the surface of sapphire. By this way, the undamaged region would appear in the sacrificial layer, and can be removed during the etching process, forming deep and connected microstructures with high aspect ratio. To make sure that the undamaged region appears in the sacrificial layer, the thickness of SiO_2 film should be larger than the depth of undamaged region. In this regard, we investigated the dependence of the depth of undamaged region and the laser fluence. Experimentally, the thickness of undamaged region increased from approximately 0.7 to 1.6 μm with laser fluence increasing from 105 to 180 J/cm^2 (Fig. 2c). Therefore, the thickness of SiO_2 film that deposited on the surface of sapphire should be larger than 2 μm. In theory, we also investigated their relationship. The simulated light intensity distribution (the

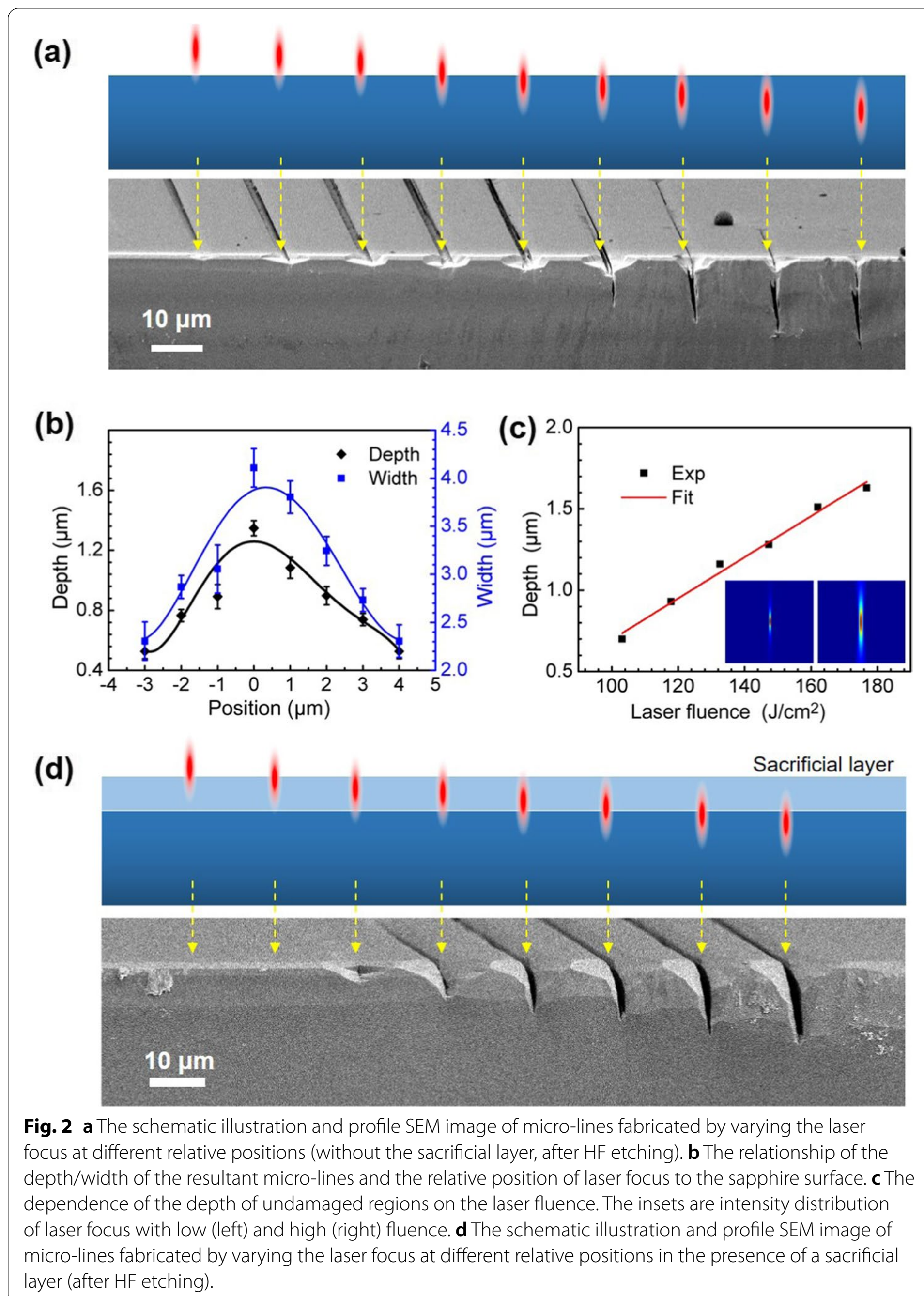

Fig. 2 **a** The schematic illustration and profile SEM image of micro-lines fabricated by varying the laser focus at different relative positions (without the sacrificial layer, after HF etching). **b** The relationship of the depth/width of the resultant micro-lines and the relative position of laser focus to the sapphire surface. **c** The dependence of the depth of undamaged regions on the laser fluence. The insets are intensity distribution of laser focus with low (left) and high (right) fluence. **d** The schematic illustration and profile SEM image of micro-lines fabricated by varying the laser focus at different relative positions in the presence of a sacrificial layer (after HF etching).

insets of Fig. 2c) shows the amplified intensity distribution length, which is agree with the experimental results. Figure 2d shows the comparable scheme and the profile SEM image of the microgrooves. In the presence of a sacrificial layer, the sapphire-air interface changes to SiO_2-air interface. As a result, sapphire grooves with high aspect ratios can be readily fabricated. Introducing a cover glass with a thickness of 150 µm has been used in inscribing waveguide near the surface. However, this method requires a higher flatness to the substrate to form Vander Waals attractive forces between the atoms of the surfaces [20, 21]. In our work, the sacrificial layer of SiO_2 was fabricated by electron

beam evaporation. The deposited SiO_2 film can eliminate the residual air in the interface which is easy to form when the substrate is not a strict flat surface.

By introducing SiO_2 as a sacrificial layer, the undamaged region would appear in the SiO_2 layer, which could be removed by HF etching. Thus, various micro/nano-structures of high aspect ratio could be fabricated on sapphire surface through an inside-out deep scribing manner. Figure 3 shows the SEM images of several typical microstructures fabricated on sapphire surface. Both the surface patterns and the section profiles of these microstructures can be designed and fabricated by programming the laser scanning path. For example, a wave lines array with a line width of 800 nm has been fabricated on ultra-hard sapphire surface using this method (Fig. 3a). Magnified SEM image shows that the surface of the wave-line structure is quite smooth, no

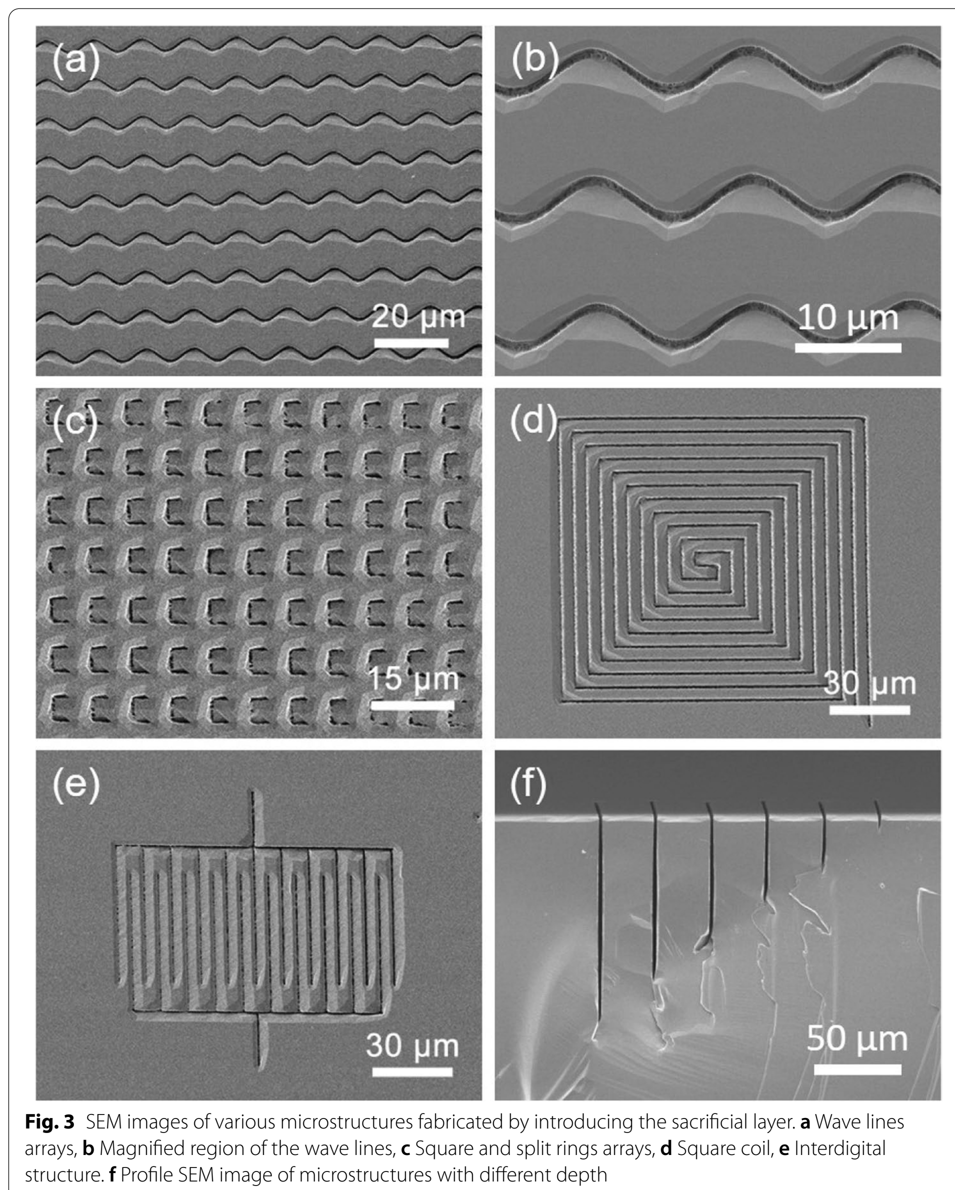

Fig. 3 SEM images of various microstructures fabricated by introducing the sacrificial layer. **a** Wave lines arrays, **b** Magnified region of the wave lines, **c** Square and split rings arrays, **d** Square coil, **e** Interdigital structure. **f** Profile SEM image of microstructures with different depth

crack and damage can be detected around it (Fig. 3b), indicating the high precision. Besides, a split ring array with an average resolution of 1 μm and a period of 8 μm has been fabricated on sapphire (Fig. 3c). Actually, taking advantage of the designable processing capability, any desired patterns can be readily produced on sapphire. Figure 3d and e demonstrate a continuous square coil structure and an interdigital structure, respectively. Through an inside-out writing manner, the depth of microstructures can be flexibly tuned by controlling the laser scanning depth. Figure 3f shows the profile of the microstructures of different depth, in which the aspect ratio as high as 80:1 has been achieved. In fact, this value can be further increased with increasing the laser scanning depth. The results indicated that this method enables fabricating high-quality microstructures with high aspect ratio on sapphire, holding great promise for biomimetic fabrication.

Inspired by the cornea of moth eye that has excellent antireflection properties, we demonstrated the fabrication of sub-wavelength antireflection structures on sapphire for optical window applications. Sapphire can act as the optical window materials in the mid-IR region owing to its high thermal, mechanical and chemical stability, and high transmittance in the IR spectral region [22, 23]. In addition to the intrinsic high transmission of the window materials, antireflection sub-wavelength structures can offer a gradient refractive index profile between two sides of the interface, which can significantly enhance the transmission [24–29]. To date, to realize structure induced transmission enhancement, various advanced technologies, for instance, electron-beam etching, laser interference, and mask lithography have been employed to fabricate sub-wavelength antireflection structures [30–35]. However, these methods are not suitable for such biomimetic fabrication on sapphire, because the high mechanical strength and chemical stability make it challenging to fabricate of sub-wavelength microstructures. Various femtosecond laser-based methods have been proposed to fabricate sapphire microstructures [36–38]. However, these methods cannot meet the requirements of infrared window structure for high resolution and high surface quality. In this work, we successfully fabricated antireflection sub-wavelength structures on sapphire using the sacrificial layer assisted inside-out deep laser scribing technology.

Figure 4a-c shows the morphology of the cornea of moth eye. On the surface of the compound eyes, there are hundreds of ommatidia closely packed on a curved surface. On each ommatidium, micropillar arrays distributed periodically on the surface. The ommatidia function as cameras, and the micropillar arrays are helpful for transmission enhancement. Inspired from this interesting structure, we designed antireflection sub-wavelength structures, pyramidal structure array with an average period of 2 μm. The parameters of the antireflection sub-wavelength structure were determined by the following formula according to the effective medium theories (EMT's) [39] (the schematic of the designed structures can be seen in Supplement 1, Fig. S1):

$$\frac{p}{\lambda} = \frac{1}{n_2 + n_1 \sin\theta_{max}} \tag{4}$$

where p is the period of antireflection sub-wavelength structures, n_2 =1.77 is the refractive index of sapphire, n_1 =1 is the refractive index of air, θ_{max} =90° is the maximum value of incident angle. Accordingly, the period of antireflection sub-wavelength

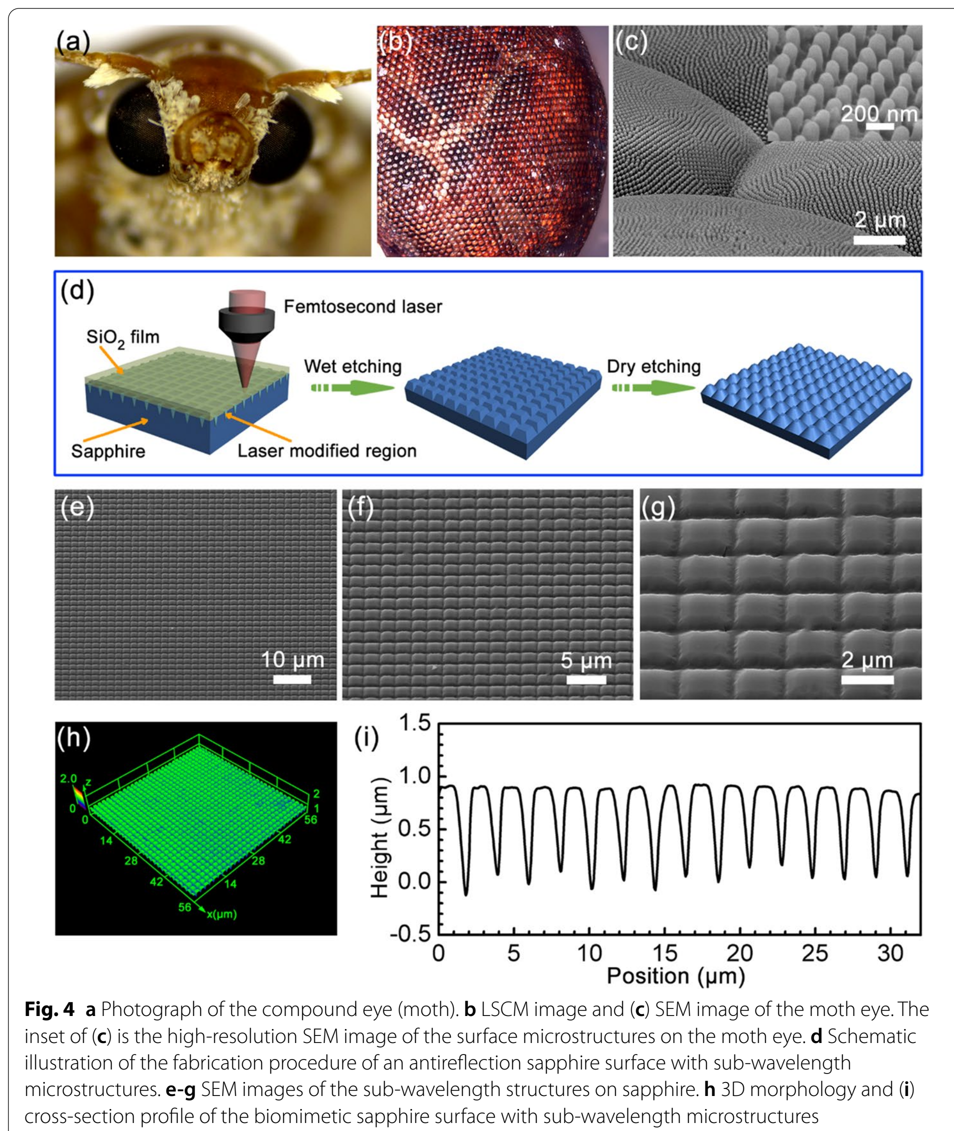

Fig. 4 **a** Photograph of the compound eye (moth). **b** LSCM image and (**c**) SEM image of the moth eye. The inset of (**c**) is the high-resolution SEM image of the surface microstructures on the moth eye. **d** Schematic illustration of the fabrication procedure of an antireflection sapphire surface with sub-wavelength microstructures. **e-g** SEM images of the sub-wavelength structures on sapphire. **h** 3D morphology and (**i**) cross-section profile of the biomimetic sapphire surface with sub-wavelength microstructures

structures should be less than 2.26 μm for a typical IR wavelength (λ) of 4 μm (popular in IR cameras).

The planar periodicity of the sub-wavelength antireflection structure determines the operating wavelength, while the height and shape of the pattern determine the antireflection performance. The optimal height of the structure (h) for a minimal reflectivity is: [39]

$$h_{min} = \frac{\lambda}{4\sqrt{n_1 n_2}} \tag{5}$$

where λ is the typical IR wavelength of 4 μm, and n_1 and n_2 are the refractive indices of sapphire and air, respectively. Thus, the height of the antireflection sub-wavelength structures should be larger than 0.75 μm. The size and height of micro/nanostructures is critical to the optical performance [40, 41]. To satisfy the requirement of the period

and the height, we employed a sacrificial layer for the inside-out laser deep scribing of sapphire. Since both the sacrificial layer and the laser modified region can be removed with the help of HF etching, the antireflection sub-wavelength structures have been successfully fabricated through our method (Fig. 4d). SEM images of the moth eye inspired antireflection sapphire window show the uniform distribution of a close-pack sub-wavelength structures over a large area (Fig. 4e-h). Magnified SEM image (Fig. 4g) confirms the good surface smoothness. Cross-section profile indicates that the height of the antireflection structure is approximately 1 μm (Fig. 4i). It is worthy pointing out that it is quite challenging to fabricate such a biomimetic antireflection structure on sapphire surface through a general femtosecond laser modification and etching method, the presence of a sacrificial layer plays the key role to achieve high-quality antireflection structures. As a control experiment, we also fabricated the same structure on sapphire under the same condition without the use of the sacrificial layer, the rough surface confirm the importance of the sacrificial layer (Fig. S2).

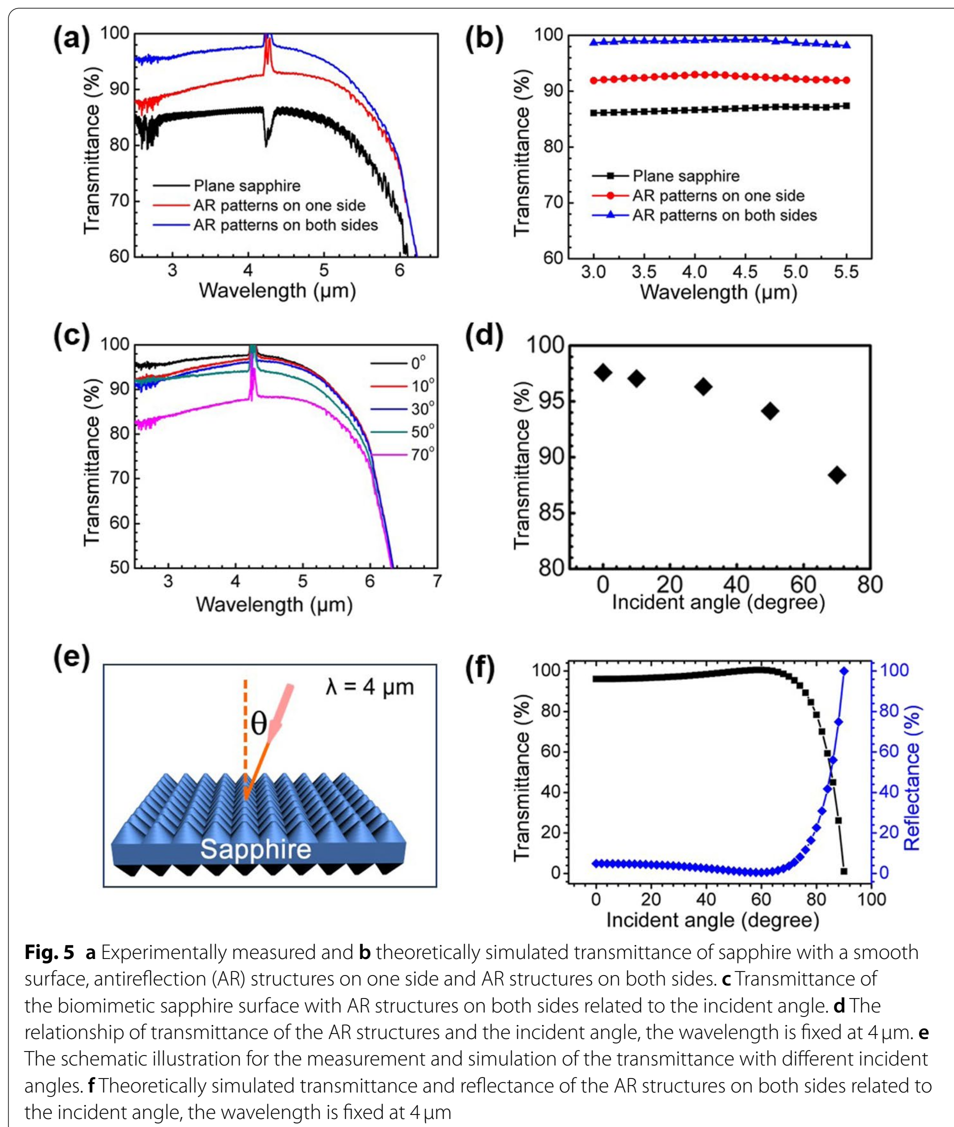

Fig. 5 **a** Experimentally measured and **b** theoretically simulated transmittance of sapphire with a smooth surface, antireflection (AR) structures on one side and AR structures on both sides. **c** Transmittance of the biomimetic sapphire surface with AR structures on both sides related to the incident angle. **d** The relationship of transmittance of the AR structures and the incident angle, the wavelength is fixed at 4 μm. **e** The schematic illustration for the measurement and simulation of the transmittance with different incident angles. **f** Theoretically simulated transmittance and reflectance of the AR structures on both sides related to the incident angle, the wavelength is fixed at 4 μm

The optical performance of the antireflection structures was investigated using Fourier transform infrared spectrometry. As compared with the pristine sapphire, the transmittance of the sapphire with antireflection structures increased significantly in the mid-infrared range from 2.5 to 6 μm (Fig. 5a). The sapphire glass with antireflection structures on both sides shows a transmittance of ~ 98% at 4 μm, and the one with antireflection structures on one side shows a transmittance of ~ 92%. Both of them are much higher than that of the plane one (86%). The theoretical simulations by VirtualLab Fusion software shows the similar value of the transmittance in the three cases (Fig. 5b), in good agreement with our experimental results. Additionally, the transmission dependence on the incidence angle was also investigated both experimentally and theoretically (Fig. 5c-f). With increasing of the incidence angle from 0 to 50°, the transmission of sapphire with antireflection structures on both sides decreased slightly, but still above 95% at 4 μm. Further increase of incidence angle to 70° would cause the obvious decrease of transmission to 89% at μm (Fig. 5c, d). The theoretical calculations for the sapphire sample with two side antireflection structures shows an angle-independent transmission and reflection up to 70° for the non-polarized light at 4 μm (Fig. 5f), which shows a similar tendency with the experimental results.

Conclusion In summary, we proposed an inside-out femtosecond laser deep scribing technology for fabricating biomimetic microstructures with high-aspect-ratio on sapphire. By introducing a sacrificial layer of SiO_2 on sapphire surface, uncontrollable surface damages and the undamaged region underneath can be effectively avoided. As a result, high-quality microstructures with a maximum aspect ratio of 80:1 have been readily produced on sapphire surface. In addition, to demonstrate the full potential of this technology in biomimetic microfabrication, a uniform pyramidal structures array inspired from the cornea of moth eye have been fabricated on sapphire. A broadband angle independent transmittance for incidence angles up to 70° and a high transmittance of ~ 98% at 4 μm have been achieved. The biomimetic sapphire processing technology may hold great promise for producing micro-optical devices that can work under harsh conditions.

Abbreviations

3D: Three-dimensional; SiO_2: Silicon oxide; HF: Hydrofluoric acid; IR: Infrared rays; ICP: Inductively coupled plasma; Cl_2: Chlorine; BCl_3: Boron trichloride; SEM: Scanning electron microscopy; LSCM: Laser scanning confocal microscopy; FTIR: Fourier transform infrared spectrometry..

Supplementary Information

The online version contains supplementary material available at https://doi.org/10.1186/s43074-022-00047-3.

Additional file 1: Figure S1. The schematic of the designed antireflection sub-wavelength pyramidal structures array. **Figure S2.** (a) SEM image, (b) optical image and (c) cross-section profile of the microstructures fabricated by etching assisted femtosecond laser modification without a sacrificial layer, respectively. The structures were nonuniform and the height of the microstructures was only approximately 300 nm.

Acknowledgements

Not applicable.

Authors' contributions

X.-Q. Liu, Q.-L. Li, and H.-B. Sun conceived the initial idea, X.-Q. Liu, Q.-L. Li, J.-X. Zheng and Y.-M. Lu performed the experiments. X.-Q. Liu analyzed the data. Y.-L. Zhang, S. Juodkazis, Q.-D. Chen, and H.-B. Sun discussed the results and supervised the project. All authors read and approved the final manuscript.

Funding
This work was supported by the National Natural Science Foundation of China (NSFC, Grant Nos. 61825502, 61960206003, 61935008 and 62105117) and the Scientific Research Project of the Education Department of Jilin Province (JJKH20221005KJ).

Availability of data and materials
The datasets used and/or analysed during the current study are available from the corresponding author on reasonable request.

Declarations

Competing interests
The authors declare that they have no competing interests.

Author details
[1]State Key Laboratory of Integrated Optoelectronics, College of Electronic Science and Engineering, Jilin University, Changchun 130012, China. [2]Centre for Micro-Photonics, Faculty of Science, Engineering and Technology, Swinburne University of Technology, Hawthorn, VIC 3122, Australia. [3]Melbourne Centre for Nanofabrication, ANFF, 151 Wellington Road, Clayton, VIC 3168, Australia. [4]State Key Laboratory of Precision Measurement Technology and Instruments, Department of Precision Instrument, Tsinghua University, Haidian, Beijing 100084, China.

Received: 22 November 2021 Accepted: 31 December 2021
Published online: 21 January 2022

References
1. Sakakura M, Lei Y, Wang L, Yu YH, Kazansky PG. Ultralow-loss geometric phase and polarization shaping by ultrafast laser writing in silica glass. Light Sci. Appl. 2020;9:15.
2. Gissibl T, Schmid M, Giessen H. Spatial beam intensity shaping using phase masks on single-mode optical fibers fabricated by femtosecond direct laser writing. Optica. 2016;3(4):448–51.
3. Liu X-Q, Yu L, Yang S-N, Chen Q-D, Wang L, Juodkazis S, et al. Optical nanofabrication of concave microlens arrays. Laser Photonics Rev. 2019;13(5):1800272.
4. Yan L, Yang D, Gong Q, Li Y. Rapid fabrication of continuous surface Fresnel microlens array by femtosecond laser focal field engineering. Micromachines. 2020;11(2):112.
5. Wang H, Zhang Y-L, Han D-D, Wang W, Sun H-B. Laser fabrication of modular superhydrophobic chips for reconfigurable assembly and self-propelled droplet manipulation. PhotoniX. 2021;2(1):1–13.
6. Jiang L, Wang AD, Li B, Cui TH, Lu YF. Electrons dynamics control by shaping femtosecond laser pulses in micro/nanofabrication: modeling, method, measurement and application. Light Sci Appl. 2018;7(2):17134.
7. Juodkazis S, Nishimura K, Misawa H, Ebisui T, Waki R, Matsuo S, et al. Control over the crystalline state of sapphire. Adv. Mater. 2006;18(11):1361–4.
8. Li Z-Z, Wang L, Fan H, Yu Y-H, Sun H-B, Juodkazis S, et al. O-FIB: far-field-induced near-field breakdown for direct nanowriting in an atmospheric environment. Light Sci. Appl. 2020;9(1):1–7.
9. Xu SZ, Sun K, Yao CZ, Liu H, Miao XX, Jiang YL, et al. Periodic surface structures on dielectrics upon femtosecond laser pulses irradiation. Opt. Express. 2019;27(6):8983–93.
10. Wang L, Xu B-B, Cao X-W, Li Q-K, Tian W-J, Chen Q-D, et al. Competition between subwavelength and deep-subwavelength structures ablated by ultrashort laser pulses. Optica. 2017;4(6):637–42.
11. Li X, Guan Y. Theoretical fundamentals of short pulse laser–metal interaction: A review. Nanotechnol Precis Eng. 2020;3(3):105–25.
12. Hu Y, Rao S, Wu S, Wei P, Qiu W, Wu D, et al. All-glass 3D optofluidic microchip with built-in tunable microlens fabricated by femtosecond laser-assisted etching. Adv. Opt. Mater. 2018;6(9):1701299.
13. Sugioka K, Cheng Y. Ultrafast lasers—reliable tools for advanced materials processing. Light: Sci Appl. 2014;3(4):e149.
14. Liu X-Q, Chen Q-D, Guan K-M, Ma Z-C, Yu Y-H, Li Q-K, et al. Dry-etching-assisted femtosecond laser machining. Laser Photonics Rev. 2017;11(3):1600115.
15. Liu X-Q, Yang S-N, Yu L, Chen Q-D, Zhang Y-L, Sun H-B. Rapid engraving of artificial compound eyes from curved sapphire substrate. Adv. Funct. Mater. 2019;29(18):1900037.
16. Deng Z, Chen F, Yang Q, Bian H, Du G, Yong J, et al. Dragonfly-eye-inspired artificial compound eyes with sophisticated imaging. Adv. Funct. Mater. 2016;26(12):1995–2001.
17. Wang C, Yang L, Zhang C, Rao S, Wang Y, Wu S, et al. Multilayered skyscraper microchips fabricated by hybrid "all-in-one" femtosecond laser processing. Microsyst. Nanoeng. 2019;5(1):1–10.
18. Lapointe J, Bérubé JP, Ledemi Y, Dupont A, Fortin V, Messaddeq Y, et al. Nonlinear increase, invisibility, and sign inversion of a localized fs-laser-induced refractive index change in crystals and glasses. Light Sci. Appl. 2020;9(1):1–12.
19. Lin J, Yu S, Ma Y, Fang W, He F, Qiao L, et al. On-chip three-dimensional high-Q microcavities fabricated by femtosecond laser direct writing. Opt. Express. 2012;20(9):10212–7.
20. Bérubé J-P, Vallée R. Femtosecond laser direct inscription of surface skimming waveguides in bulk glass. Opt. Lett. 2016;41(13):3074–7.
21. Bérubé J-P, Frayssinous C, Lapointe J, Dupont A, Vallée R. Direct inscription of near-surface waveguides in crystals, glasses, and polymers (Conference Presentation), Frontiers in Ultrafast Optics: Biomedical, Scientific, and Industrial Applications XX. Int Soc Optics Photonics. 2020;11270:112700R.

22. Schubert M, Tiwald TE, Herzinger CM. Infrared dielectric anisotropy and phonon modes of sapphire. Phys Rev B. 2000;61(12):8187.
23. Harris DC, Johnson LF, Seaver R, Lewis T, Turri G, Bass M, et al. Optical and thermal properties of spinel with revised (increased) absorption at 4 to 5 μm wavelengths and comparison with sapphire. Opt Eng. 2013;52(8):087113.
24. Clapham PB, Hutley MC. Reduction of lens reflexion by the "Moth Eye" principle. Nature. 1973;244(5414):281–2.
25. Vukusic P, Sambles JR. Photonic structures in biology. Nature. 2003;424(6950):852–5.
26. Zhang G, Zhang J, Xie G, Liu Z, Shao H. Cicada wings: a stamp from nature for nanoimprint lithography. Small. 2006;2(12):1440–3.
27. Huang YF, Chattopadhyay S, Jen YJ, Peng CY, Liu TA, Hsu YK, et al. Improved broadband and quasi-omnidirectional anti-reflection properties with biomimetic silicon nanostructures. Nat Nanotec. 2007;2(12):770–4.
28. Min WL, Jiang B, Jiang P. Bioinspired self-cleaning antireflection coatings. Adv Mater. 2008;20(20):3914–8.
29. Rahman A, Ashraf A, Xin H, Tong X, Sutter P, Eisaman MD, et al. Sub-50-nm self-assembled nanotextures for enhanced broadband antireflection in silicon solar cells. Nat Commun. 2015;6(1):1–6.
30. Wang L, Xu B-B, Chen Q-D, Ma Z-C, Zhang R, Liu Q-X, et al. Maskless laser tailoring of conical pillar arrays for antireflective biomimetic surfaces. Opt Lett. 2011;36(17):3305–7.
31. Sun CH, Min WL, Linn NC, Jiang P, Jiang B. Templated fabrication of large area subwavelength antireflection gratings on silicon. Appl Phys Lett. 2007;91(23):231105.
32. Zhao Y, Wang J, Mao G. Colloidal subwavelength nanostructures for antireflection optical coatings. Opt Lett. 2005;30(14):1885–7.
33. Wang S, Yu XZ, Fan HT. Simple lithographic approach for subwavelength structure antireflection. Appl Phys Lett. 2007;91(6):061105.
34. Liao Y, Pan W, Cui Y, Qiao L, Bellouard Y, Sugioka K, et al. Formation of in-volume nanogratings with sub-100-nm periods in glass by femtosecond laser irradiation. Opt Lett. 2015;40(15):3623–6.
35. Li X, Hu XK, Li YF, Chai L. A three-step procedure for the design of broadband terahertz antireflection structures based on a subwavelength pyramidal-frustum grating. J Lightwave Technol. 2013;32(8):1463–71.
36. Mazilu M, Juodkazis S, Ebisui T, Matsuo S, Misawa H. Structural characterization of shock-affected sapphire. Applied Physics A. 2007;86(2):197–200.
37. Hörstmann-Jungemann M, Gottmann J, Keggenhoff M. 3D-Microstructuring of Sapphire using fs-Laser Irradiation and Selective Etching. J Laser Micro/Nanoengineering. 2010;5(2):145–9.
38. Liu H, Li Y, Lin W, Hong M. High-aspect-ratio crack-free microstructures fabrication on sapphire by femtosecond laser ablation. Optics Laser Technology. 2020;132:106472.
39. Raguin DH, Morris GM. Antireflection structured surfaces for the infrared spectral region. Appl Opt. 1993;32(7):1154–67.
40. Zou X, Zheng G, Yuan Q, Zang W, Chen R, Li T, et al. Imaging based on metalenses. PhotoniX. 2020;1(1):1–24.
41. Ding X, Wang Z, Hu G, Liu J, Zhang K, Li H, et al. Metasurface holographic image projection based on mathematical properties of Fourier transform. PhotoniX. 2020;1(1):1–12.

Publisher's Note

Springer Nature remains neutral with regard to jurisdictional claims in published maps and institutional affiliations.

Submit your manuscript to a SpringerOpen journal and benefit from:

- Convenient online submission
- Rigorous peer review
- Open access: articles freely available online
- High visibility within the field
- Retaining the copyright to your article

Submit your next manuscript at ▶ springeropen.com